Supporting information

N vacancies modulated Zn single atoms for efficient H_2O_2 photosynthesis

Wenke Xie, [a] Junyu Liu, [a] Xuan-He Liu,*[a]

[a] *School of Science, China University of Geosciences (Beijing), Beijing 100083. China.*

* Corresponding author: liuxh@cugb.edu.cn

Experimental sections

Chemicals

Melamine, Zinc chloride, ethanol, Cerium (IV) sulfate tetrahydrate and Sodium sulfate. were purchased from Innochem technology and used without further purification.

Characterization

The X-ray powder diffraction pattern (XRD) of the photocatalysts were collected by using the PANalytical Empyrean. To obtain the morphology of materials, the transmission electron microscope (TEM) and HRTEM images were measured on a JEM-2100F electron microscope. An aberration-corrected high-angle annular dark-field scanning TEM (AC-HAADF-STEM) characterization was acquired on a JEM ARM200F thermal field emission microscope. The mass fractions of Zn were determined by ICP-OES (Agilent ICP-OES 5110). UV-vis absorption spectroscopy was performed on UV2600 UV-vis spectrophotometer with $BaSO_4$ as the standard. Fourier transform infrared (FT-IR) spectroscopy was taken on the IR Affinity-1 FTIR spectrometer (Shimadzu, Japan). X-ray photoelectron spectroscopy (XPS) was employed using a ESCALab250Xi instrument. Photoluminescence (PL) properties were implemented on Horiba FluoroMax PLUS fluorescence spectrophotometer with 350 nm excitation. Electron paramagnetic response (EPR) spectra were recorded on a Bruker E500 at room temperature. The coordination environments of Zn atoms were obtained by using x-ray absorption fine structure (XAFS) spectroscopy at the Beijing Synchrotron Light Source (BSRF) operating at 1W1B station (operated at 2.5 GeV).

Photoelectrochemical measurements

Photoelectrochemical measurements were tested in 0.5 M Na_2SO_4 aqueous solution on a CHI660E electrochemical workstation with a typical three-electrode system. A 300 W Xe lamp was used as the simulated light source, and Ag/AgCl and Pt electrodes were used as the reference and counter electrodes, respectively. A slurry was made by ultrasonically mixing 5 mg of catalyst dispersed in 1 mL of anhydrous ethanol and 10 μL of Nafion solution for 30 min, which was then added dropwise onto FTO glass (1×1 cm^2) as a working electrode. The instantaneous photocurrent densities were determined by light on/off cycling under light irradiation at 0.4 V (vs. Ag/AgCl). Also, the electrochemical impedance spectra (EIS) were recorded in the range of $0.01 \sim 10^5$ Hz at the same bias voltage. The Mott-Schottky plots were acquired at a frequency of 1000 Hz and an amplitude of 10 mV.

Photocatalytic H_2O_2 production

10 mg of photocatalyst was dispersed in a mixed solution containing 95 mL water and 5 mL ethanol. The suspension was dispersed homogeneously by ultrasound, while at the same time O_2 was bubbled in the suspension to saturate the reaction environment with O_2. A 300 W Xe lamp (Perfect Light PLS-SEX 300) equipped with an AM1.5G filter was used as a simulated illumination (240 ± 5 $mW \cdot cm^{-2}$). The concentration of H_2O_2 was measured by UV-VIS spectrophotometer. For example, 2 mL liquid sample was taken from the reactor and was filtered through a 0.22 μm filter to remove the photocatalyst, and then mixed with pre-prepared 1 mM $Ce(SO_4)_2$ solution. The UV spectrophotometric $Ce_2(SO_4)_3$ colorimetry method follows formula (1), in which yellow Ce^{4+} can be reduced by H_2O_2 to form colorless Ce^{3+}.

$$2Ce^{4+} + H_2O_2 \rightarrow 2Ce^{3+} + 2H^+ + O_2 \qquad (1)$$

The concentration of H_2O_2 can be calculated from equation (2):

$$c(H_2O_2) = ½ \times c(Ce^{4+}) \quad (2)$$

To obtain the calibration curve, a known concentration of H_2O_2 was added to $Ce(SO_4)_2$ solution and the change in absorption intensity was measured by UV/Vis spectrometer. Based on the linear relationship between Ce^{4+} concentration and signal intensity, the H_2O_2 concentration of the photocatalyst can be calculated as follows:

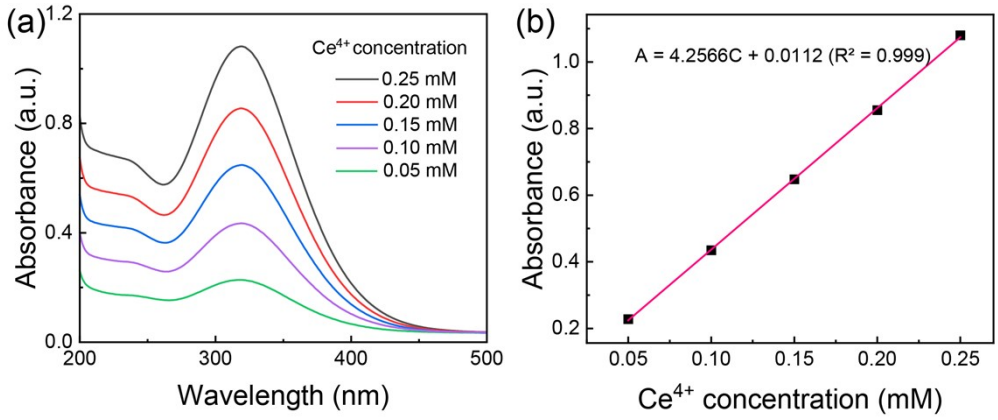

The apparent quantum yields of the photocatalysts were determined under 300 W Xenon lamp. The active area of the photocatalytic reactor is about 15.9 cm^2. Monochromatic light intensities were averaged at five representative points using a PL-MW2000 photoradiometer. The light intensities at 350, 375, 400, and 425 nm were 7.6, 20.4, 29.9, and 35.0 mW/cm^2, respectively. Then, the AQY was calculated using the equation (3) as follows:

$$\eta_{AQY} = = \frac{2 \times h \times n \times N_A \times c}{S \times P \times t \times \lambda} \times 100\% \quad (3)$$

n, the Number of H_2O_2 molecules (mol); h, Planck constant (6.626×10^{-34} JS); N_A, Avogadro constant (6.022×10^{23} mol^{-1}); c, the speed of light (3×10^8 m/s); S, the active area of the photocatalytic reactor (cm^2); P, irradiation intensity ($W \cdot cm^{-2}$); t, photoreaction time (s); λ, filter wavelength (m).

Rotating disk electrode (RDE) measurements

The substrate of the working electrode is a glassy carbon rotating disk electrode. 2 mg photocatalyst was dispersed in 500 μL containing 10 μL Nafion solution (5 wt%) by ultrasonication. 50 μL of the above slurry was placed on a disk electrode and dried at room temperature. Ag/AgCl and Pt wire electrode were used as reference and counter electrode respectively. The linear scanning voltammetric curve (LSV) was recorded at room temperature in O_2 saturated 0.1 M phosphate buffer solution (pH = 7.2) at a scanning rate of 10 $mV \cdot s^{-1}$ at different rotational speeds. Using Koutecky-Levich equation to calculate the average number of electrons (n), equation (4) and (5) as follows [1, 2]:

$$\frac{1}{J} = \frac{1}{J_L} + \frac{1}{J_K} = \frac{1}{(B \times W^{1/2})} + \frac{1}{J_K} \quad (4)$$

$$B = 0.2nFC_0D_0^{2/3}V^{-1/6} \quad (5)$$

J, current density; J_K and J_L, kinetic and diffusion-limited current density; ω, the rotation speed (rpm); F, Faraday constant (96485 $C \cdot mol^{-1}$); n, electron transfer number; C_o, bulk concentration of O_2 (1.26×10^{-6} $mol \cdot cm^{-3}$); v, the kinetic viscosity of the electrolyte (0.01 $cm^2 \cdot s^{-1}$); D_o, diffusion coefficient of O_2 (2.7×10^{-5} $cm^2 \cdot s^{-1}$).

Rotating ring-disk electrode (RRDE) measurement

The working electrode was prepared similarly to the RDE measurement method. Voltammograms were obtained in 0.1 M phosphate buffer solution (pH = 7.2) at a scan rate of 10 $mV \cdot s^{-1}$ with a rotation rate of 1000 rpm at room temperature.

Theoretical calculation details

Theoretical calculations were carried out by using the Quickstep algorithm of *CP2K (version 2023.2)* package.[3] Two-dimensional models of Zn-CN and Zn-CN_{2nd} were constructed and optimized to an energy-minimal geometry. The unit size was expanded to 26.6 and 23.7 Å of each dimension, and a vacuum slab of 30 Å was placed above each system. The structural optimization was performed using Perdew-Burke-Ernzerhof (PBE) functional[4] with the Grimme's dispersion correction with Becke-Johnson damping (D3BJ) [5, 6]. The plane wave methods, a double-ζ polarization quality Gaussian basis sets (DZVP-MOLOPT-SR-GTH) and a 400 Ry plane wave cutoff for the auxiliary grid were used. A convergence criterion of 3.0×10^{-6} a.u. was used for the optimization of the wave function. The Brillouin zone of these systems was sampled by gamma-point due to the large unit size. The model construction and input/output file process were supported by *Multiwfn (version 3.8dev)* package.[7]

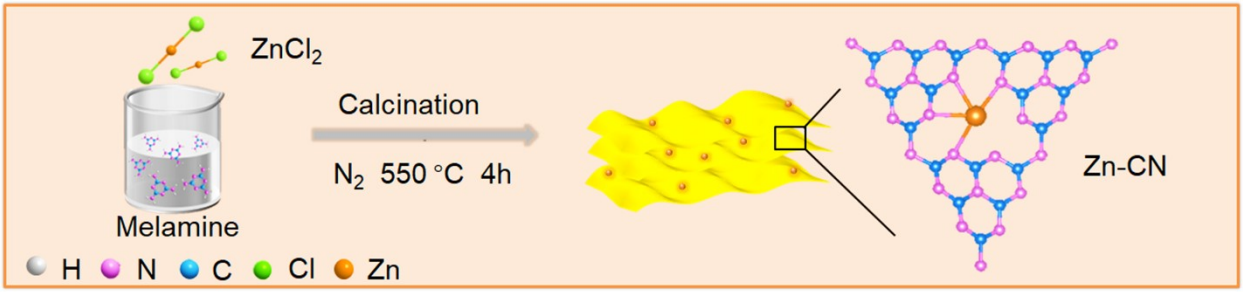

Fig. S1 Schematic synthesis of Zn-CN.

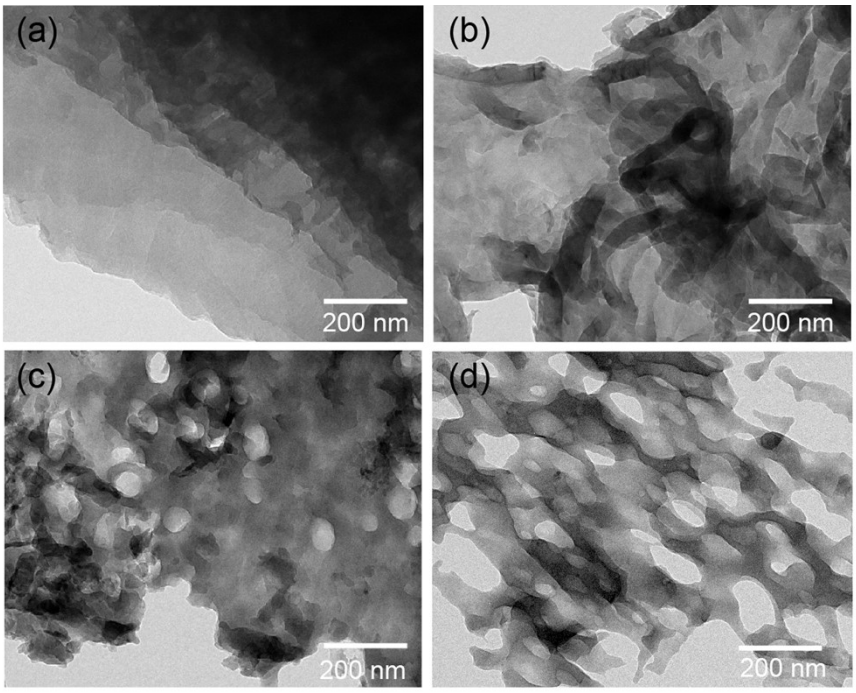

Fig. S2 TEM images of CN, CN_{2nd}, Zn-CN and Zn-CN_{2nd}.

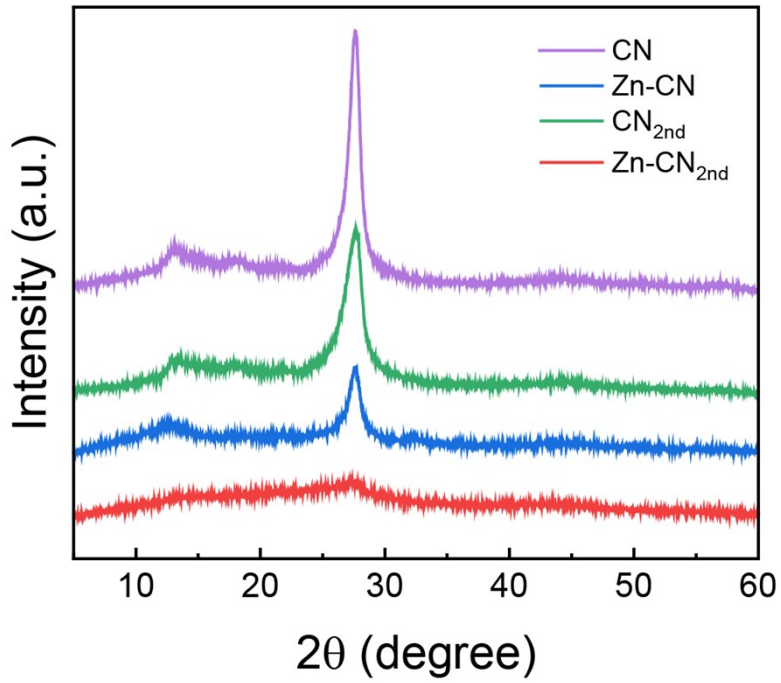

Fig. S3 XRD patterns of CN, CN_{2nd}, Zn-CN and Zn-CN_{2nd}.

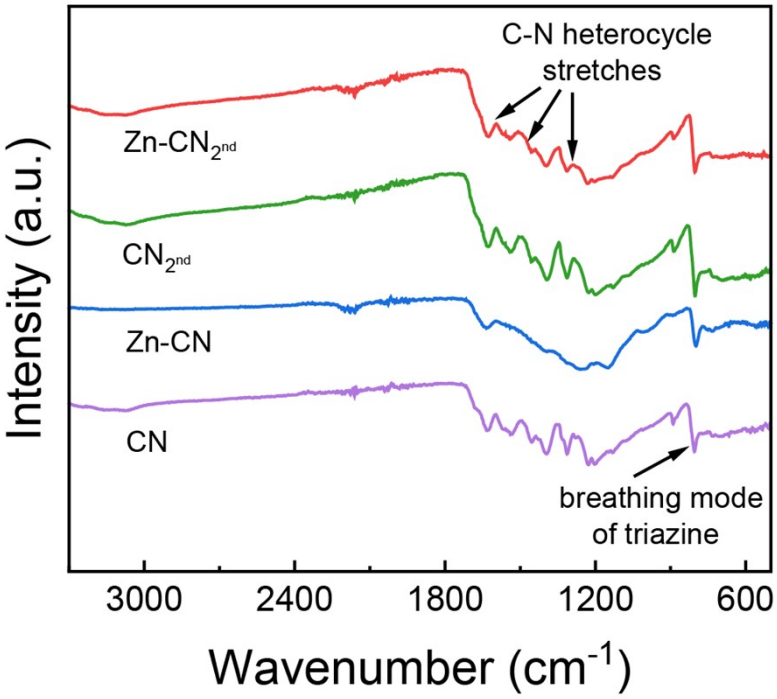

Fig. S4 FT-IR spectra of CN, CN_{2nd}, Zn-CN and Zn-CN_{2nd}.

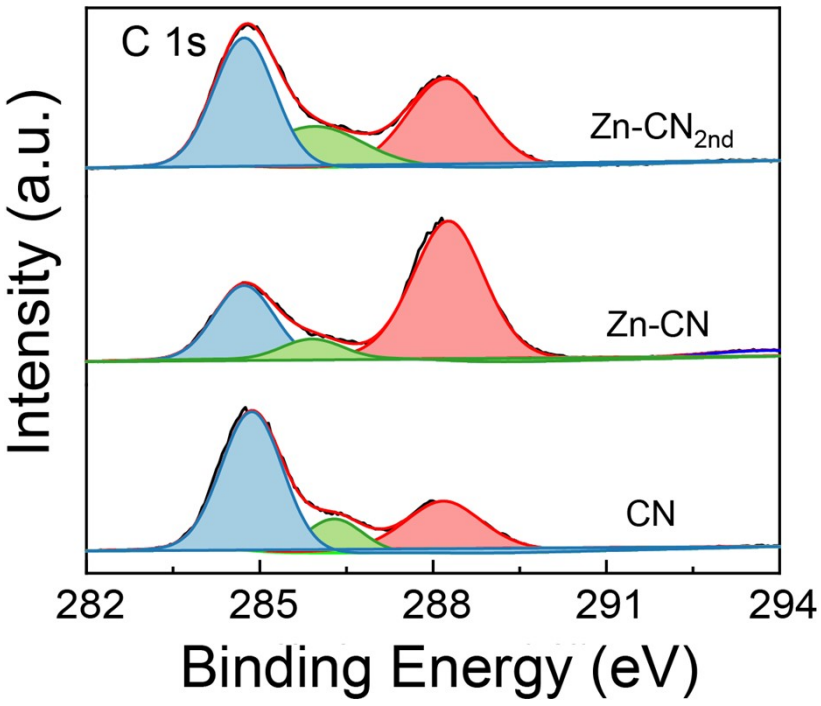

Fig. S5 The high-resolution C 1s XPS spectra of CN, Zn-CN and Zn-CN_{2nd}.

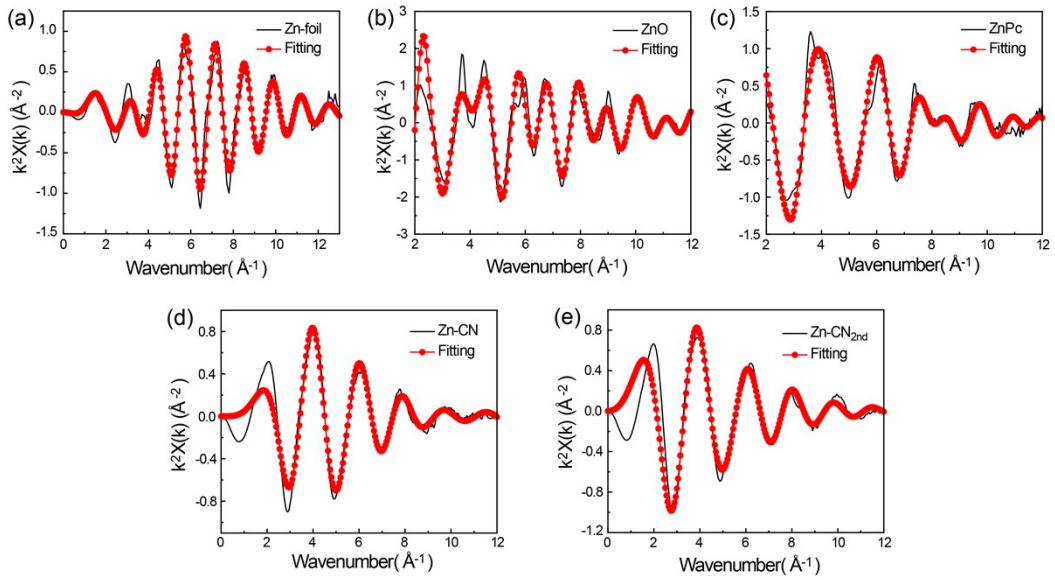

Fig. S6 Extended X-ray absorption fine structure (EXAFS, k^2-weighted k-space) of (a) Zn foil, (b) ZnO, (c) ZnPc, (d) Zn-CN and (e) Zn-CN_{2nd}.

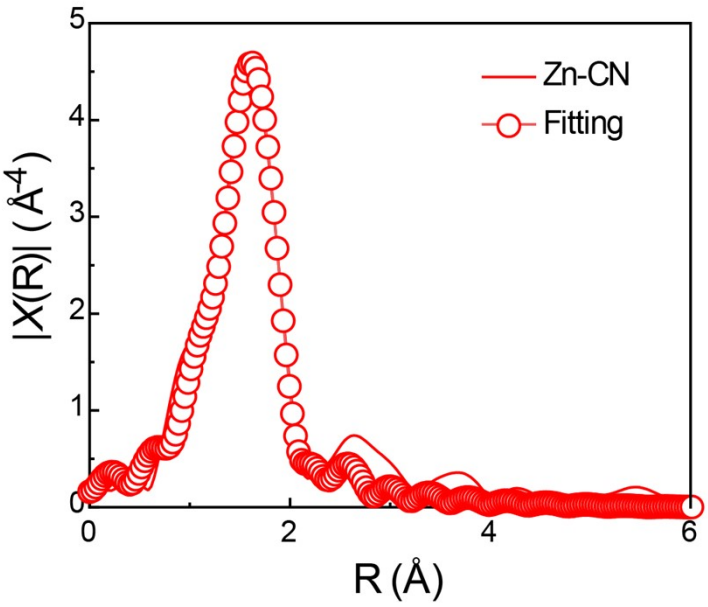

Fig. S7 Zn K-edge EXAFS fitting results of Zn-CN.

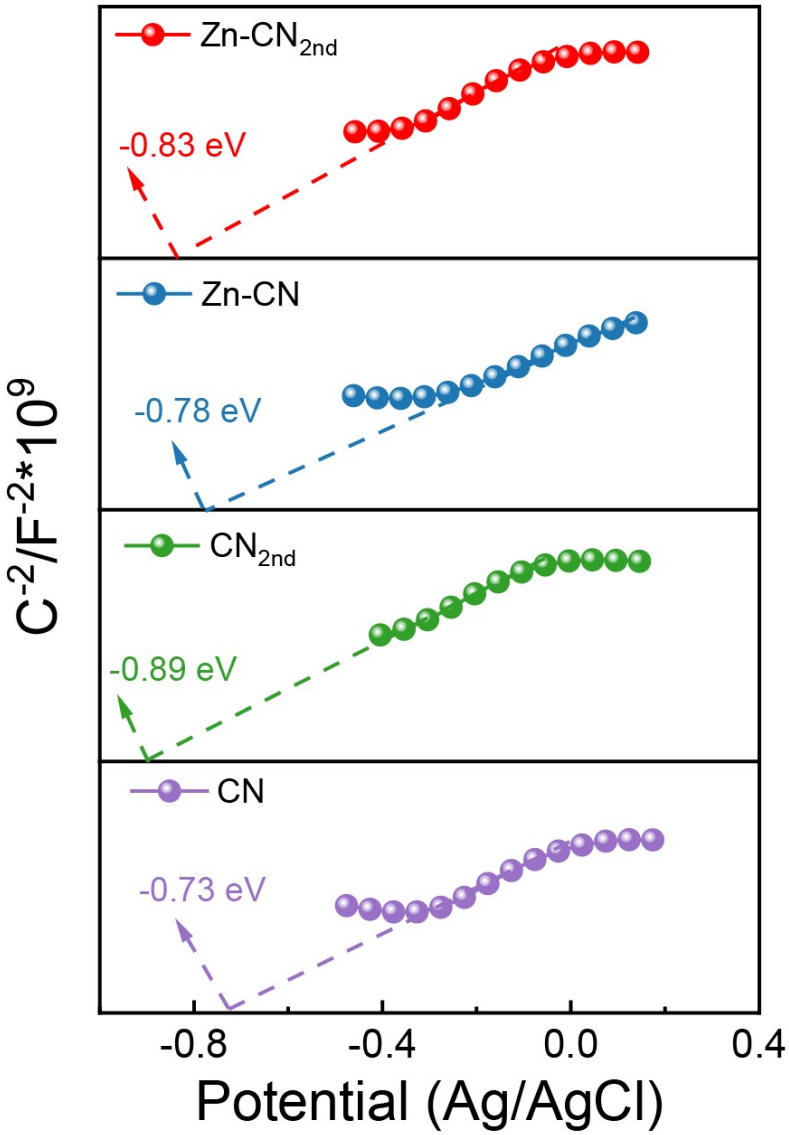

Fig. S8 Mott–Schottky plots of CN, CN_{2nd}, Zn-CN and Zn-CN_{2nd}.

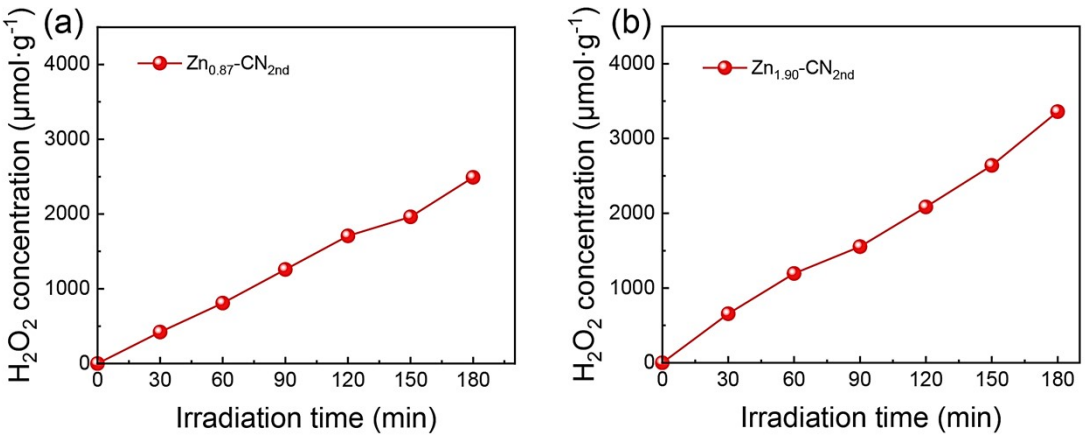

Fig. S9 (a) Photocatalytic H_2O_2 yield of $Zn_{0.87}$-CN_{2nd} and $Zn_{1.90}$-CN_{2nd}.

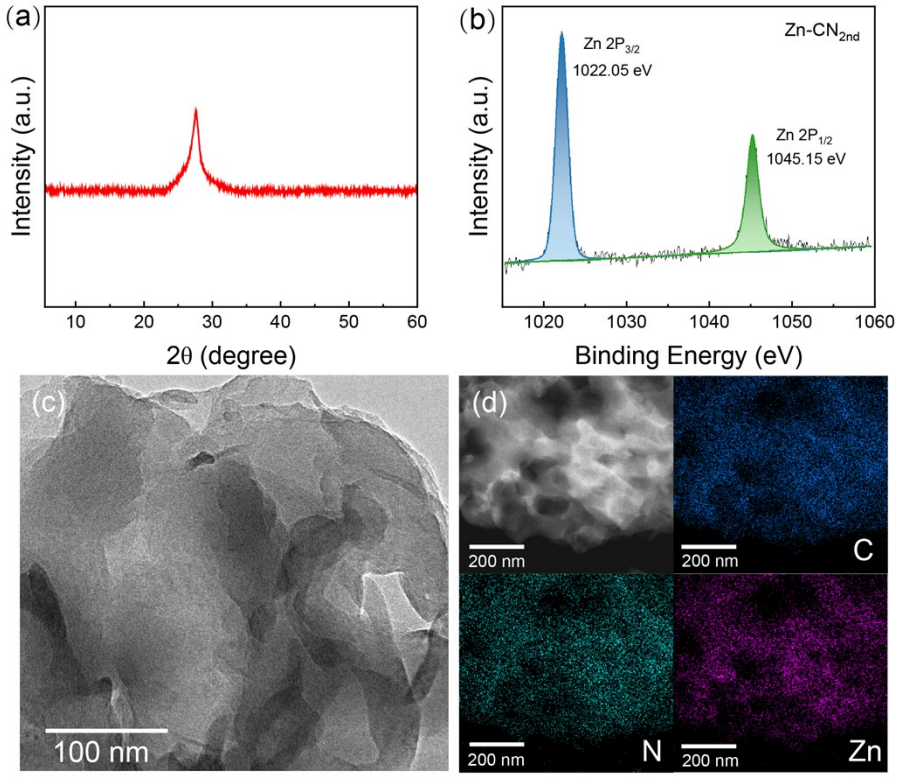

Fig. S10 (a) XRD pattern, (b) Zn 2p XPS spectra, (c) TEM image, and (d) EDS images of Zn-CN_{2nd} after the cycling test.

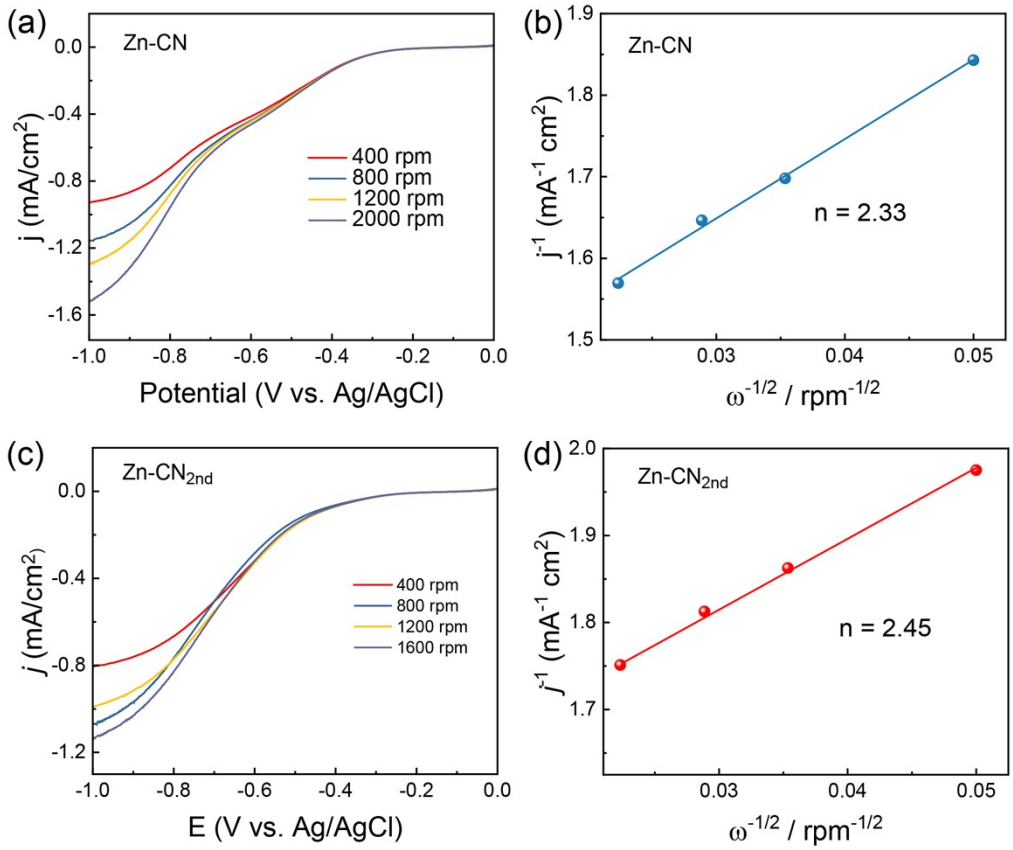

Fig. S11 Linear sweep voltammogram (LSV) curves of (a) Zn-CN and (c) Zn-CN_{2nd} were measured in O_2-saturated 0.1 M phosphate buffer solution at different rotational speeds. Koutecky–Levich plots of (b) Zn-CN and (d) Zn-CN_{2nd} obtained from RDE measurements.

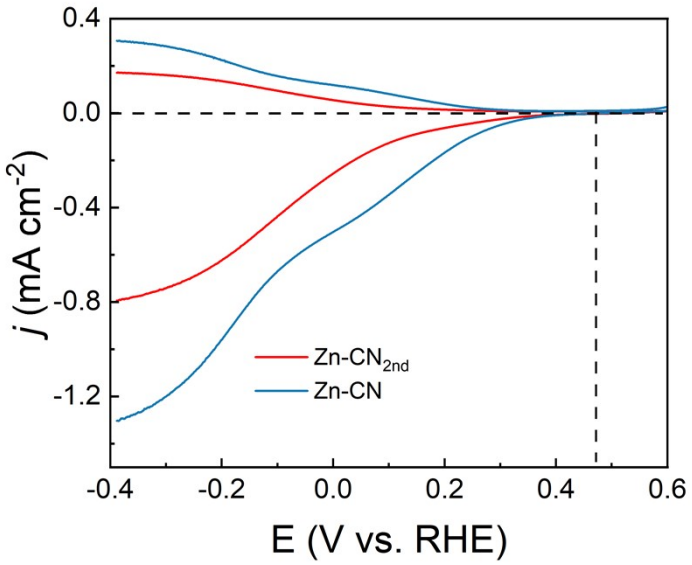

Fig. S12 Polarization curves of Zn-CN and Zn-CN_{2nd} were recorded at 1000 rmp in 0.1 M phosphate-buffered saline during simultaneous detection of H_2O_2 at the ring electrode.

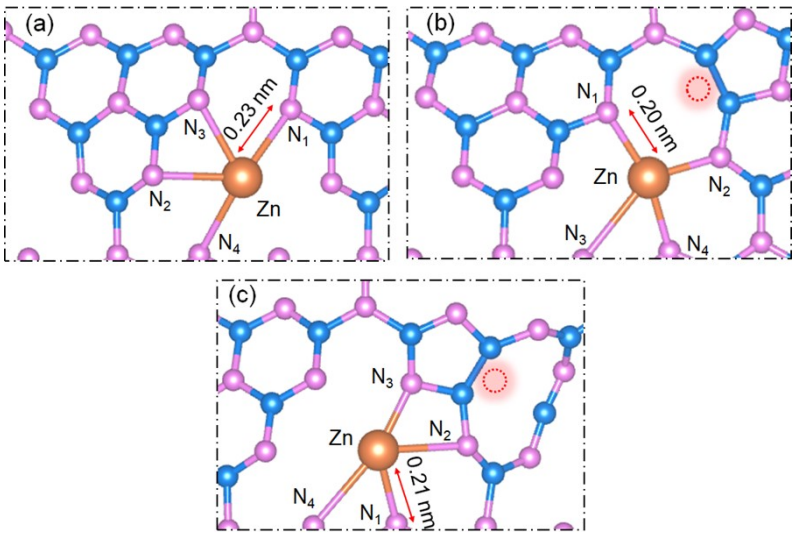

Fig. S13 Calculated structure models of (a) Zn-CN, (b) Zn-$CN_{2nd\text{-}I}$ and (c) Zn-$CN_{2nd\text{-}II}$.

Table1. Element analysis of the different samples

Sample	C:N
Zn-CN	2.09
Zn-CN_{2nd}	1.99

Table S2. EXAFS fitting parameters at the Zn *K*-edge for Zn-CN, Zn-CN_{2nd}, Zn foil, ZnO and ZnPc.

Sample	Path	N	ΔE(eV)	100xR(Å)	$10^3x\sigma^2$(Å^2)	R-factor
Zn-foil	Zn-Zn_1	6	1.33(0.28)	264.0(0.5)	11.02(2.25)	0.002
	Zn-Zn_2	6	7.80(1.26)	318.2(1.2)	9.25(2.69)	
ZnO	Zn-O	4	3.51(1.71)	196.5(1.3)	3.40(0.35)	0.006
	Zn-Zn	12	2.25(0.75)	323.3(0.3)	5.25(1.26)	
ZnPc	Zn-N	4	8.44(1.29)	208.5(1.2)	8.62(1.32)	0.007
	Zn-C	4	4.31(1.12)	296.3(1.3)	4.72(1.22)	
Zn-CN	Zn-N	4.19(0.24)	6.36(0.98)	205.6(1.9)	8.02(0.53)	0.008
ZN-CN_{2nd}	Zn-N	4.39(0.38)	2.21(0.13)	202.4(1.4)	9.88(1.22)	0.006

N, coordination number; *R*, distance between absorber and backscatter atoms; σ^2, Debye-Waller factor to account for both thermal and structural disorders; ΔE, inner potential correction; R factor indicates the goodness of the fit. S_0^2 was fixed to 0.79. A reasonable range of EXAFS fitting parameters: $0.600 < S_0^2 < 1.000$; $\sigma^2 > 0$ Å^2; $|\Delta E_0| < 15$ eV.

Table S3. Comparison of photocatalytic performance of H_2O_2 production of Zn-CN_{2nd} catalyst with C_3N_4-based photocatalysts

Catalyst	Irradiation condition	H_2O_2 $\mu mol \cdot g^{-1} \cdot h^{-1}$	Reaction solution, catalyst amount	Ref.
Zn-CN_{2nd}	AM 1.5G	1363.4	100 mL 5 vol% EtOH, 10 mg	This work
NDCN	300 W Xe lamp ($\lambda \geq 420$ nm)	476.0	100 mL 10 vol% IPA, 100 mg	[8]
CN4	300 W Xe lamp ($\lambda \geq 420$ nm)	574.0	100 mL 10 vol% IPA, 50 mg	[9]
Ti_3C_2/g-C_3N_4	300 W Xe lamp ($\lambda \geq 420$ nm)	1317	50 mL 10 vol% IPA, 50 mg	[10]
Homo-CN	300 W Xe lamp ($\lambda \geq 420$ nm)	508.4	50 mL 10 vol% EtOH, 50 mg	[11]
PCN	300 W Xe lamp ($\lambda \geq 420$ nm)	1071.7	25 mL 10 vol% IPA, 20 mg	[12]
fl-CN-530	300 W Xe lamp ($\lambda \geq 420$ nm)	952.3	50 mL 10 vol% EtOH, 10 mg	[13]
$SCBCN_{0.4}$	300 W Xe lamp ($\lambda \geq 420$ nm)	620.2	100 mL 10 vol% EtOH, 40 mg	[14]

References for SI:

[1]. L. Chen, L. Wang, Y. Wan, Y. Zhang, Z. Qi, X. Wu, H. Xu, *Adv. Mater.* 2020, **32** (2), 1904433.

[2]. J. Gao, B. Liu, *ACS Mater. Lett.* 2020**, 2** (8), 1008-1024.

[3]. T. D. Kühne, M. Iannuzzi, M. Del Ben, V. V. Rybkin, P. Seewald, F. Stein, T. Laino, R. Z. Khaliullin, O. Schütt, F. Schiffmann, D. Golze, Jan Wilhelm, S. Chulkov, M. H. Bani-Hashemian, V. Weber, U. Borštnik, M.Taillefumier, A. S. Jakobovits, A. Lazzaro, H. Pabst, T. Müller, R. Schade, M. Guidon, S. Andermatt, N. Holmberg, G. K. Schenter, A. Hehn, A. Bussy, F. Belleflamme, G. Tabacchi, A. Glöß, M. Lass, I.Bethune, C. J. Mundy, C. Plessl, M. Watkins, J. VandeVondele, M. Krack, J. Hutter, 2020, **152** (19). 194103.

[4]. J. P. Perdew, K. Burke, M. Ernzerhof, *Phys Rev Lett.* 1996, **77** (18), 3865.

[5]. S. Grimme, J. Antony, S. Ehrlich, H. Krieg, *J. Chem. Phys.* 2010**, 132** (15), 154104.

[6]. S. Grimme, S. Ehrlich, L. Goerigk, *J. Comput. Chem.* 2011, **32** (7), 1456-1465.

[7]. T. Lu, F. Chen, *J. Comput. Chem.* 2012, **33** (5), 580-592.

[8]. J. Luo, Y. Liu, C. Fan, L. Tang, S. Yang, M. Liu, M. Wang, C. Feng, X. Ouyang, L. Wang, L. Xu, J. Wang, M. Yan, *ACS Catal.* 2021, **11** (18), 11440-11450.

[9]. C. Feng, L. Tang, Y. Deng, J. Wang, J. Luo, Y. Liu, X. Ouyang, H. Yang, J. Yu, J. Wang, *Adv. Funct. Mater.* 2020, **30**, 2001922.

[10]. Y. Yang, Z. Zeng, G. Zeng, D. Huang, R. Xiao, C. Zhang, C. Zhou, W. Xiong, W. Wang, M. Cheng, W. Xue, H. Guo, X. Tang, D. He, *Appl. Catal. B Environ.* 2019**, 258**, 117956.

[11]. Q. Chen, C. Lu, B. Ping, G. Li, J. Chen, Z. Sun, Y. Zhang, Q. Ruan, L. Tao, *Appl. Catal. B Environ.* 2023**, 324**, 122216.

[12]. L. Xu, L. Li, Z. Hu, J. C. Yu, *Appl. Catal. B Environ.* 2023**, 328,** 122490.

[13]. B. Feng, Y. Liu, K. Wan, S. Zu, Y. Pei, X. Zhang, M. Qiao, H. Li, B. Zong, *Angew. Chem. Int. Ed.* 2024, **63**, e202401884.

[14]. Q. You, C. Zhang, M. Cao, B. Wang, J. Huang, Y. Wang, S. Deng, G. Yu, *Appl. Catal. B Environ.* 2023**, 321**, 121941.